Robotica (2016) volume 34, pp. 2788–2805. © Cambridge University Press 2015
doi:10.1017/S0263574715000399

Spherical trigonometry constrained kinematics for a dexterous robotic hand with an articulated palm

Evangelos Emmanouil†, Guowu Wei‡ and Jian S. Dai§,*

†*Centre for Robotics Research, Department of Informatics, King's College London, University of London, Strand, London WC2R 2LS, UK. Email: evangelos.emmanouil@kcl.ac.uk*
‡*School of Computing, Science, and Engineering, University of Salford, The Crescent, Salford, Manchester M5 4WT, UK. Email: g.wei@salford.ac.uk*
§*Chair of Mechanisms and Robotics, Centre for Robotics Research, Department of Informatics, King's College London, Uuniversity of London, Strand, London WC2R 2LS, UK.*

(Accepted May 11, 2015. First published online: June 17, 2015)

SUMMARY
This work presents a method based on spherical trigonometry for computing all joint angles of the spherical metamorphic palm. The spherical palm is segmented into spherical triangles which are then solved and combined to fully solve the palm configuration. Further, singularity analysis is investigated with the analysis of each spherical triangle the palm is decomposed. Singularity-avoidance-based design criteria are then presented. Finally, point clouds are generated that represent the joint space of the palm as well as the workspace of the hand with the advantage of an articulated palm is shown.

KEYWORDS: Robotic hand; Spherical five-bar linkage; Spherical mechanism; Metamorphic mechanism; Reconfigurable mechanism; Origami inspired; Kinematics; Workspace; Joint space.

1. Introduction

Dexterous robotic hands are a topic that attracted a lot of attention since the milestone development of the Stanford/Jet Propulsion Laboratory (JPL) hand and the Massachusetts Institute of Technology (MIT)/Utah hand in the early of 1980s.[1] Since then, a number of multifingered robotic hands have been designed and developed all over the world. They include, to name but a few, the prosthetic hand-based Belgrade/University of Southern California (USC) hand[2] which incorporated a thumb and two more coupled pairs of fingers that adapted to the shape of the grasped object and so the whole hand needed only four motors while it had five digits; the highly integrated Deutsches Zentrum für Luft- und Raumfahrt (DLR)-Hand[3] incorporating purpose built linear actuators, position sensors both for the motors and joints, tactile sensors on each finger link, stereo camera on the palm and two axis torque sensors at the finger tips; the Robonaut hand[4,5] designed to be similar in size and capability to an astronaut's hand in a suit as well as withstand the environment of space; the tendon-driven Shadow Robot Hand[6] with a one-Degrees Of Freedom (DOF) articulated palm and a structure closely resembling the human hand with the option to either use electric motors or pneumatic artificial muscles; the self-contained three-fingered Barrett hand[7] with one finger fixed on the palm and two fingers able to rotate around the palm; the low-cost easy-to-use Laboratory of Robotics and Mechatronics in Cassino (LARM) hand[8,9] with three one-DOF fingers having each finger's joints coupled by four-bar linkages designed to mimic a human performing a cylindrical grasp; the UB hand[10,11] which has explored many novel control and actuation concepts including a twisted string actuator where by twisting two strings a rotary motion is converted to a linear one; the DLR/Harbin Institute of Technology (HIT) II hand[12] which consists of a palm module and finger modules with actuators and control system integrated in each module, and the Sungkyunkwan University (SKKU) hand[13] which also uses identical finger modules each with its own integrated control system an motors as well as six-DOF force–torque sensors at the fingertips. All these hands, anthropomorphic

* Corresponding author. E-mail: jian.dai@kcl.ac.uk

or non-anthropomorphic, are capable of performing certain degree of dexterous motions. However, they are either based on a rigid palm, or the degree to which the palm can be articulated is limited to splitting the palm into two or three pieces such that the workspace and dexterity of these hands are limited.

In order to reduce the limitations and provide robotic hands with greater workspace and additional dexterity and versatility, a novel metamorphic robotic hand was invented and developed by Dai and his colleagues[14–17] based on the concept of metamorphosis[18] stemming from origami folding.[19,20] The novelty of the metamorphic robotic hand lies in the introduction of an articulated palm which is formed by a spherical metamorphic linkage that provides the palm capability of changing mobility, topology and configuration. This articulated palm design enables the new robotic hand to perform and emulate more complex and sophisticated hand motions. It also allows the hand to be fully folded to pass through tight spaces and to change its configuration to adapt to various task requirements. Therefore, a thorough investigation of the articulated palm plays a critical role in the kinematics, dynamics, control and application of the novel metamorphic hand.

Spherical linkages, the linkages that have the property that every link in the system rotates about the same fixed point, have been widely investigated and used by mathematicians, mechanicians and engineers. Liu and Ting[21] established rotatability criteria for spherical chains based on rotatability laws for planar linkages. Gosselin and Hamel[22] developed the agile eye based on a spherical parallel mechanism. In order to investigate the kinematics of spherical mechanisms, Wampler[23] formulated loop equations to solve the kinematics of parallel spherical mechanisms up to three loops. McCarthy[24] used structure equations together with trigonometric constraints to analyse the kinematics of serial and closed-loop spherical linkages. Gupta and Beloiu[25] proposed algebraic-geometrical methods to eliminate branch and circuit defects in the synthesis of spherical four-bar linkages. Chiang[26] has also carried out significant work on the analysis of spherical mechanisms but primarily focuses on spherical four-bar linkages. Duffy[27] used spherical trigonometry to solve geared five-bar linkages of mobility $M = 1$ and provided the inspiration that leads to the work presented in this paper.

Using loop equations Cui and Dai,[28] and Wei *et al.*[17] investigated kinematics, workspace and manipulability of the metamorphic robotic hand. However, the work presented in refs. [17–28] focused only on the direct or forward kinematics of the metamorphic robotic hand. Further, there was no differentiation of the reflex and non-reflex coupler joint configurations.

By using the spherical trigonometry, a solution for the forward and inverse kinematics of the metamorphic palm is derived that does not involve solving a system of complicated trigonometry equations that are difficult to understand intuitively. Thus, the process is less prone to human error compared to solving a system of a large number of equations, such as the one produced when using quaternions, the Denavit–Hartenberg (D–H) method or the loop closure method. Further, the proposed method does not involve quadratic equations which leads to loss of the sign information of the joint angles thus making identification of the reflex and non-reflex coupler joint configurations difficult. By using the spherical trigonometry, this paper presents an intuitive method that preserves joint angle sign information for workspace and joint space analysis of the reconfigurable palm of the King's College London (KCL) metamorphic hand. In turn, this provides background work for the path planning and control of the proposed metamorphic hand.

2. Geometry and Coordinate Systems

The novelty of the metamorphic hand lies in the introduction of the articulated/reconfigurable palm that enables the multifingered robotic hand to have a greater scope of producing various grasping poses. Therefore, a thorough investigation of the palm plays a critical role in solving the kinematics, dynamics, control and application of the whole hand. This paper focuses on the kinematics issue of the metamorphic hand especially on the kinematics of the articulated palm based on spherical trigonometry. The method presented herein is mainly based on the cosine and sine laws for spherical triangles.

Figure 1 shows the skeleton of the spherical five-bar linkage used for the palm. We assume that the radius of the five-bar linkage is $r = 1$ so that the length of each link will be expressed by a value in radiants. This conserves generality since every spherical mechanism can be projected onto the surface of a unit sphere, performing the calculations as described in this paper leading to the results with the actual geometry of the mechanism.

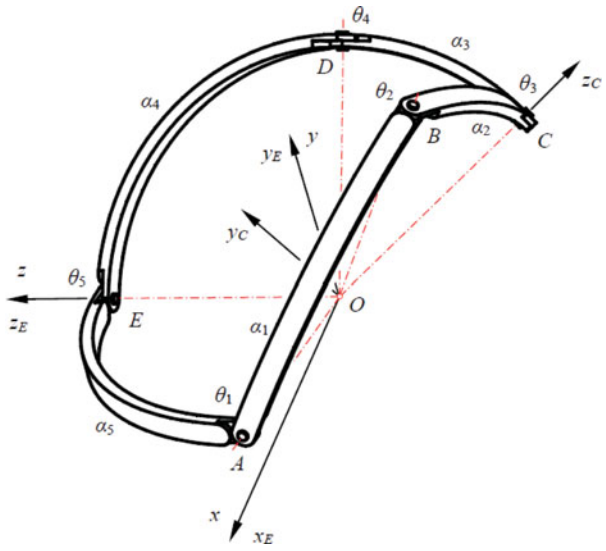

Fig. 1. Example of a spherical five-bar linkage.

The mechanism consists of five spherical links with their lengths denoted as a_1 to a_5. The links are joined by five revolute joints with their angles denoted as θ_1 to θ_5 and the rotation axes of all the revolute joints intersect at point O shown in Fig. 1. θ_1 is the crank input joint angle, θ_2 is the crank-coupler joint angle, θ_3 is the coupler joint angle, θ_4 is the coupler-rocker joint angle and θ_5 is the rocker input joint angle. In the linkage, the joints are numbered such that when all links lie on the same plane and, the first joint on each link in a counter-clockwise direction shares the same link number. Each link is assigned a reference frame denoted as F_A to F_E. The Z_i-axis (i stands for A, B, C, D and E) of each frame originates at the spherical centre O and goes through the pivot axis of the joint with the same link number. The X_i-axis is on the plane formed by the two link joints and the spherical centre O and its positive direction is on the half plane that contains the second joint. The Y_i-axis is determined by the right-hand rule and so if the mechanism was to lie on a table with the links in a counter-clockwise direction. Further, a global(reference) coordinate system $\{x, y, z\}$ is established with is origin located at point O, z-axis aligned with axis of joint E, and its y-axis directed along $Z_E \times Z_A$.

The method presented focuses on the cosine law for spherical triangles. The spherical mechanism that is the palm of the hand is decomposed into triangles. Their angles are then combined to compute the direct and inverse kinematics of the palm. This method is dealing with spherical five-bar kinematic chains of mobility $M = 2$ and the following characteristics:

$$0 < \alpha_i < \pi$$

where α_i with $i = 1, 2, 3, 4, 5$ are the angles of each link.

3. Reflex and Non-Reflex Joint-Coupler Configurations

The novel contribution of this work, is the ability to differentiate the reflex and non-reflex joint-coupler configurations. There are three possible configurations for the coupler links. The trivial straight configuration and the reflex and non-reflex configurations. In the straight configuration, the coupler joint angle is $\theta_3 = 0$. In the reflex configuration, it is $\pi/2 < \theta_3 < 2\pi$ and in the non-reflex configuration it is $0 < \theta_3 < \pi/2$. This is accomplished by the application of spherical trigonometry which allows to solve the kinematics of the palm without the use of quadratic equations, as is done in previous works.[17,28]

3.1. Position analysis and joint axis

Using the spherical five-bar mechanism shown in Fig. 1, it can be shown that each of the three output joints can be computed by an appropriate spherical triangle segmentation of the mechanism followed

https://doi.org/10.1017/S0263574715000399 Published online by Cambridge University Press

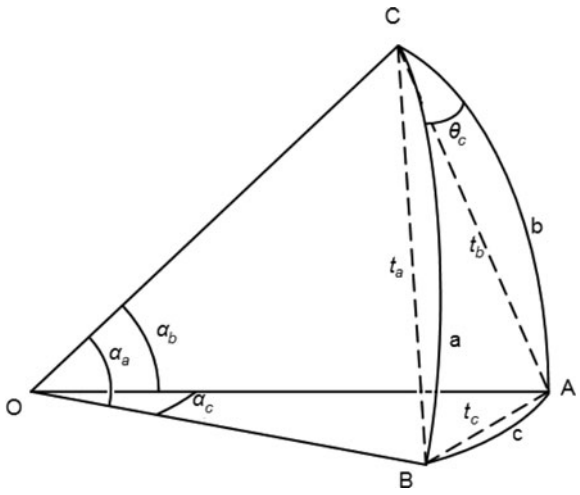

Fig. 2. A spherical triangle.

by application of the spherical cosine law with an appropriate adaptation of its terms as

$$\cos\theta_c = \frac{\cos\alpha_c - \cos\alpha_a \ \cos\alpha_b}{\sin\alpha_a \ \sin\alpha_b} \tag{1}$$

where, angles α_a and α_b correspond to the links forming the joint under consideration. Angle α_c corresponds to a third, virtual, link that completes the spherical triangle and angle θ_c is the (dihedral) joint angle being calculated, as is shown in Fig. 2.

The lengths of the adjacent links are known by the geometry of the spherical mechanism. The length of the hypothetical link can be computed by applying Eq. (2) on the chord joining the other ends of the two links under consideration. The distance between those ends can be computed by the geometry and configuration of the mechanism.

$$\alpha_c = \cos^{-1}\left(1 - \frac{t_c^2}{2}\right) \tag{2}$$

The computation of coupler joint-angle θ_3 when the input joints are θ_1 and θ_5 is a direct application of Eqs. (1) and (2), as can be seen in Eqs. (11), (26), (29) and (32). However, computing of crank-coupler joint-angle θ_2 and rocker–coupler joint angle θ_4 involves dividing the joints into more, well-defined triangles and then combining them.

So as to construct the formulae based on Eq. (2), the coordinates of the points A, B, C, D and E as well as joint angles θ_2, θ_3 and θ_4 should be computed first. We start by assuming that point E is $\boldsymbol{p}_e = [0, 0, 1]$. Then the coordinates of points A, B and D are computed and expressed by the input joint angles θ_5 and θ_1. Then, angle θ_3 can be computed by applying the cosine law for spherical triangles on the triangle $\triangle BCD$. Computing rocker–coupler joint angle θ_4 can be done by combining dihedral angles θ_{eda}, θ_{adb}, θ_{bdc} and subtracting them from π. Crank-coupler joint Angle θ_2 can be computed in a similar way, by combining θ_{abe}, θ_{ebd}, θ_{dbc} and subtracting them from π. This indicates that the chords t_{bd}, t_{be} and t_{ad} have to be computed.

Referring to Fig. 1, the coordinates for points A, B, D and E can be computed by performing the rotations described as follows.

$$\boldsymbol{p}_a = R_y(\alpha_5)\,\boldsymbol{k} \tag{3}$$

$$\boldsymbol{p}_b = R_y(\alpha_5)\,R_z(\theta_1)\,R_y(\alpha_1)\,\boldsymbol{k} \tag{4}$$

$$\boldsymbol{p}_d = R_z(-\theta_5)\,R_y(-\alpha_4)\,\boldsymbol{k} \tag{5}$$

$$\boldsymbol{p}_e = \boldsymbol{k} \tag{6}$$

https://doi.org/10.1017/S0263574715000399 Published online by Cambridge University Press

where $\boldsymbol{k} = [\,0 \quad 0 \quad 1\,]^T$. $R_y(\alpha_i)$ and $R_z(\theta_i)$ are standard rotation matrices as follows.

$$R_y(\alpha_i) = \begin{bmatrix} \cos\alpha_i & 0 & \sin\alpha_i \\ 0 & 1 & 0 \\ -\sin\alpha_i & 0 & \cos\alpha_i \end{bmatrix} \tag{7}$$

$$R_z(\theta_i) = \begin{bmatrix} \cos\theta_i & -\sin\theta_i & 0 \\ \sin\theta_i & \cos\theta_i & 0 \\ 0 & 0 & 1 \end{bmatrix} \tag{8}$$

3.2. Position analysis for cords of spherical links

Next, the chords t_{bd}, t_{be}, t_{ad} and the arc angles α_{bd}, α_{be} and α_{ad} can be calculated as follows based on Eq. (2).

Positions of $\boldsymbol{p}_b$ and $\boldsymbol{p}_d$ in Eqs. (4) and (5) yields chord t_{bd} as

$$\boldsymbol{p}_{bd} = \boldsymbol{p}_b - \boldsymbol{p}_d \tag{9}$$

$$t_{bd} = \sqrt{\boldsymbol{p}_{bd}^T\, \boldsymbol{p}_{bd}} \tag{10}$$

Substituting Eq. (10) into Eq. (2) results in

$$\alpha_{bd} = \cos^{-1}\left(1 - \frac{{t_{bd}}^2}{2}\right) \tag{11}$$

Similarly, positions of $\boldsymbol{p}_b$ and $\boldsymbol{p}_e$ in Eqs. (4) and (6) lead to chord t_{be} as

$$\boldsymbol{p}_{be} = \boldsymbol{p}_b - \boldsymbol{p}_e \tag{12}$$

$$t_{be} = \sqrt{\boldsymbol{p}_{be}^T\, \boldsymbol{p}_{be}} \tag{13}$$

Substituting Eq. (13) into Eq. (2) brings

$$\alpha_{be} = \cos^{-1}\left(1 - \frac{{t_{be}}^2}{2}\right) \tag{14}$$

Further, positions of $\boldsymbol{p}_a$ and $\boldsymbol{p}_d$ in Eqs. (3) and (5) yield chord t_{ad} as

$$\boldsymbol{p}_{ad} = \boldsymbol{p}_a - \boldsymbol{p}_d \tag{15}$$

$$t_{ad} = \sqrt{\boldsymbol{p}_{ad}^T\, \boldsymbol{p}_{ad}} \tag{16}$$

Substituting Eq. (16) into Eq. (2) results in

$$\alpha_{ad} = \cos^{-1}\left(1 - \frac{{t_{ad}}^2}{2}\right) \tag{17}$$

3.3. Spherical segregation

The pivots of the spherical five-bar linkage form a number of spherical triangles. With the values of arc angles α_{bd}, α_{be} and α_{ad} obtained above, referring to Fig. 1, dihedral angles θ_{eda}, θ_{ead}, θ_{aeb}, θ_{abe}, θ_{adb}, θ_{ebd}, θ_{dbc}, θ_{bdc} and θ_{bcd}, which are directly related to the joint angles θ_2, θ_3 and θ_4, can be formulated.

https://doi.org/10.1017/S0263574715000399 Published online by Cambridge University Press

First, the cosine law for spherical triangles is applied to every triangle under consideration. If the magnitude of the cosine of any of the triangle angles evaluates as larger than one, then the configuration is unsolvable. This would be either due to a singularity or the length of the links of the mechanism not being large enough. Next, the sine law for spherical triangles is applied. This allows solving for angles greater than π. Ultimately, the arctangent is used to derive the angle values. It is important to note that when implemented on a computer, the function Atan2 should be used, which provides the correct result when the angle is $k\,\pi$, $k \in \mathbb{N}^+$.

To prepare to solve for the rocker–coupler angle θ_{edc} and crank-coupler angle θ_{abc}, dihedral angles θ_{ead} and θ_{aeb} first need to be computed.

$$\theta_{ead} = Atan2\left(\sin\alpha_4 \frac{\sin\theta_5}{\sin\alpha_{ad}}, \frac{\cos\alpha_4 - \cos\alpha_5\ \cos\alpha_{ad}}{\sin\alpha_5\ \sin\alpha_{ad}}\right) \tag{18}$$

$$\theta_{aeb} = Atan2\left(\sin\alpha_1 \frac{\sin\theta_1}{\sin\alpha_{be}}, \frac{\cos\alpha_1 - \cos\alpha_5\ \cos\alpha_{be}}{\sin\alpha_5\ \sin\alpha_{be}}\right) \tag{19}$$

Next, rocker–coupler angle θ_{edc} segments are computed.

$$\begin{cases} \theta_{eda} = Atan2\left(\sin\alpha_5 \dfrac{\sin\theta_5}{\sin\alpha_{ad}}, \dfrac{\cos\alpha_5 - \cos\alpha_4\ \cos\alpha_{ad}}{\sin\alpha_4\ \sin\alpha_{ad}}\right) & (20) \\ \theta_{adb} = Atan2\left(\sin\alpha_1 \dfrac{\sin(\theta_1 - (-\theta_{ead}))}{\sin\alpha_{bd}}, \dfrac{\cos\alpha_1 - \cos\alpha_{ad}\ \cos\alpha_{bd}}{\sin\alpha_{ad}\ \sin\alpha_{bd}}\right) & (21) \\ \theta_{bdc} = \cos^{-1}\left(\dfrac{\cos\alpha_2 - \cos\alpha_3\ \cos\alpha_{bd}}{\sin\alpha_3\ \sin\alpha_{bd}}\right) & (22) \end{cases}$$

Crank-coupler angle θ_{abc} segments are then computed.

$$\begin{cases} \theta_{abe} = Atan2\left(\sin\alpha_5 \dfrac{\sin\theta_1}{\sin\alpha_{be}}, \dfrac{\cos\alpha_5 - \cos\alpha_1\ \cos\alpha_{be}}{\sin\alpha_1\ \sin\alpha_{be}}\right) & (23) \\ \theta_{ebd} = Atan2\left(\sin\alpha_4 \dfrac{\sin(\theta_5 - (-\theta_{aeb}))}{\sin\alpha_{bd}}, \dfrac{\cos\alpha_4 - \cos\alpha_{be}\ \cos\alpha_{bd}}{\sin\alpha_{be}\ \sin\alpha_{bd}}\right) & (24) \\ \theta_{dbc} = \cos^{-1}\left(\dfrac{\cos\alpha_3 - \cos\alpha_2\ \cos\alpha_{bd}}{\sin\alpha_2\ \sin\alpha_{bd}}\right) & (25) \end{cases}$$

Finally, coupler dihedral angle θ_{bcd} is computed.

$$\theta_{bcd} = \cos^{-1}\left(\frac{\cos\alpha_{bd} - \cos\alpha_2\ \cos\alpha_3}{\sin\alpha_2\ \sin\alpha_3}\right) \tag{26}$$

3.4. Reflex and non-reflex coupler-joint configurations

The coupler links can have two distinct configurations, as shown in Fig. 3. Previous works by Cui and Wei[17,28] presented the workspace of the metamorphic hand but did not differentiate the reflex from the non-reflex coupler-joint configurations. The difference between the two configurations is with respect to the value of the coupler joint angle being greater or less than π. In the first case, coupler joint angle θ_3 is less than π and is thus entitled as the coupler non-reflex configuration, as show in Fig. 3(a). In the case where the coupler joint angle θ_3 is larger than π, the mechanism is in the reflex coupler joint configuration, as shown in Fig. 3(b).

https://doi.org/10.1017/S0263574715000399 Published online by Cambridge University Press

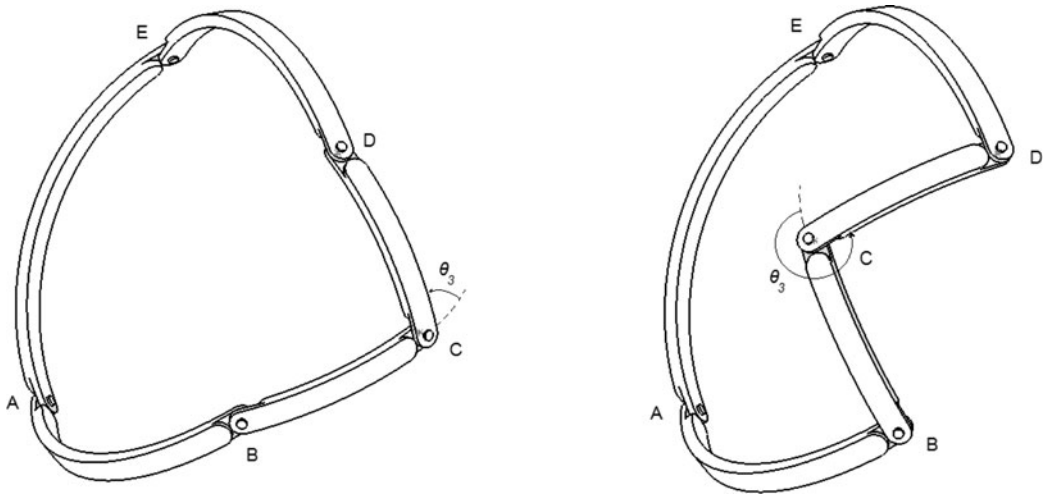

Fig. 3. Coupler non-reflex and reflex configurations. (a) CAD drawing, coupler non-reflex configuration. (b) CAD drawing, coupler reflex configuration.

To compute the output joint angles in the reflex configuration, the triangle angles are combined as follows.

$$\theta_{4r} = \pi - (\theta_{eda} + \theta_{adb} - \theta_{bdc}) = f_{4r}(\theta_1, \theta_5) \tag{27}$$

$$\theta_{2r} = \pi - (\theta_{abe} + \theta_{ebd} - \theta_{dbc}) = f_{2r}(\theta_1, \theta_5) \tag{28}$$

$$\theta_{3r} = \pi + \theta_{bcd} = f_{3r}(\theta_1, \theta_5) \tag{29}$$

In the non-reflex coupler joint configuration, it is

$$\theta_{4nr} = \pi - (\theta_{eda} + \theta_{adb} + \theta_{bdc}) = f_{4nr}(\theta_1, \theta_5) \tag{30}$$

$$\theta_{2nr} = \pi - (\theta_{abe} + \theta_{ebd} + \theta_{dbc}) = f_{2nr}(\theta_1, \theta_5) \tag{31}$$

$$\theta_{3nr} = \pi - \theta_{bcd} = f_{3nr}(\theta_1, \theta_5) \tag{32}$$

where the number in the subscript denotes the angle index number and the letter in the subscript denotes the reflex or non-reflex coupler joint configuration.

To obtain the inverse kinematics for the palm, the same set of equations is used with a simple cyclic permutation of the arc and dihedral joint angles, as long as the given dihedral joint angles are adjacent. For example, if values for θ_3 and θ_4 are given, the following permutations are necessary.

$$\begin{pmatrix} \theta_3 & \theta_4 & \theta_5 & \theta_1 & \theta_2 \\ \theta_5 & \theta_1 & \theta_2 & \theta_3 & \theta_4 \end{pmatrix}$$

and

$$\begin{pmatrix} a_3 & a_4 & a_5 & a_1 & a_2 \\ a_5 & a_1 & a_2 & a_3 & a_4 \end{pmatrix}$$

where θ_i are the dihedral joint angles of the mechanism and a_i are the arc lengths corresponding to each link of the mechanism.

4. Singularities

The main contribution of this work in terms of singularity analysis are the cases where the mechanism is singular, but can still be controlled. Common CAD software fails to simulate the mechanism when the axis of any of the joints become co-linear. A solution is presented on how to deal with this

https://doi.org/10.1017/S0263574715000399 Published online by Cambridge University Press

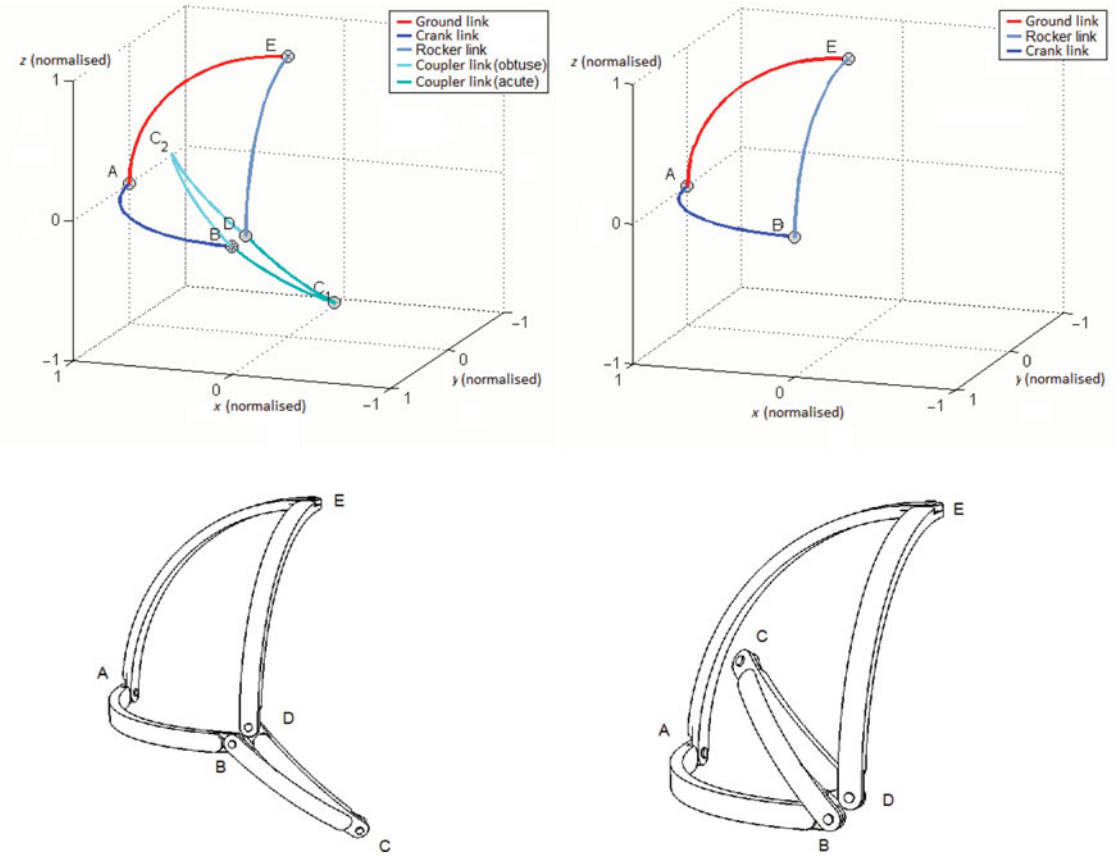

Fig. 4. Singular configuration. (a) Approaching a singularity. (b) Singular configuration. (c) Approaching a singularity, CAD drawing, coupler-non-reflex-angle. (d) Approaching a singularity, CAD drawing, coupler-reflex-angle.

problem. First, the singularity conditions are presented, followed by singularity avoidance design criteria and lastly, the singular but controllable cases are presented with a simple solution.

The singular configurations become apparent when inspecting the outcome of applying the cosine law to the spherical triangles, as indicated in Section 3. A singularity occurs when two joints axes are collinear. However, loss of control happens only when both collinear joints are output joints. If the two joints happen to be one output and one input joint, then the mechanism can still be controllable as a one-DOF mechanism. Equations (18) to (25) reveal these exact singularities of the linkage.

Figure 4(b) illustrates this singular configuration by using a spherical mechanism with link angles $\alpha_4 = \alpha_5 = \alpha_1 = \frac{\pi}{2}$ and $\alpha_2 = \alpha_3 = \frac{\pi}{4}$ and joint angles $\theta_1 = 90$ and $\theta_5 = 90$. Link AE is the ground link. Link AB is the crank and link DE is the rocker. Links B_iC_i and C_iD_i are the two possible configurations for the couplers. At the singular configuration, points B and D overlap, joint angle $\theta_3 = k\,\pi$, $k \in N^+$ and joint angles θ_2 and θ_4 are undefined. The normalization in Fig. 4(b) has been carried out in such a way that all the arcs fall on the unit sphere. This is achieved by multiplying each link length by a_i/l_i where a_i is the arc angle in radiants of the ith link and l_i is the length in meters of the ith link.

4.1. Singularity avoidance based design criteria

In particular, to avoid a singularity all of the following conditions must be met.

$$\sin a_{AD} \neq 0 \tag{33}$$

$$\sin a_{BE} \neq 0 \tag{34}$$

$$\sin a_{BD} \neq 0 \tag{35}$$

https://doi.org/10.1017/S0263574715000399 Published online by Cambridge University Press

which can be further refined to the next three conditions

$$t_{AD} \neq 0, 2 \tag{36}$$

$$t_{BE} \neq 0, 2 \tag{37}$$

$$t_{BD} \neq 0, 2 \tag{38}$$

However, loss of control only occurs in the case where $t_{BD} = 0 or 2$. In order to avoid the possibility of a singular configuration which can lead to loss of control, the following design criteria must be met:

$$\alpha_2 \neq \alpha_3 \tag{39}$$

$$\alpha_4 + \alpha_5 - \alpha_1 \neq \pi \tag{40}$$

$$\alpha_1 + \alpha_5 - \alpha_4 \neq \pi \tag{41}$$

$$\alpha_1 + \alpha_4 < \alpha_5 \tag{42}$$

$$\alpha_1 + \alpha_4 + \alpha_5 < 2\pi \tag{43}$$

4.2. The one-DOF singular but solveable case

Another contribution of this work is the solution for the case the palm is singular but controllable. In the case where the two collinear axes are one input and one output axis, the mechanism is still controllable but reduces to one DOF. In such a case, the following change happens in the kinematics Eqs. (31), (28), (30), and (27)

$$\theta_{abe} + \theta_{ebd} = \begin{cases} \pi - \theta_5 & \text{if } t_{AD} = 0 \\ \theta_5 & \text{if } t_{AD} = 2 \end{cases} \tag{44}$$

$$\theta_{eda} + \theta_{adb} = \begin{cases} \pi - \theta_1 & \text{if } t_{BE} = 0 \\ \theta_1 & \text{if } t_{BE} = 2 \end{cases} \tag{45}$$

5. Workspace of the Palm of the KCL Multifingered Metamorphic Robotic Hand

The method presented in this paper, is used to visualise the joint space of the KCL metamorphic hand. The joint space of the KCL Metamorphic hand is generated by varying the two input angles across all possible angle positions with a step of 2°. Then all joint angles for the output angles when the palm is not in a non-singular configuration are recorded.

5.1. Position analysis of the joint-coupler of the palm

Finally, point C can be located by either following the E, D, C path, as seen in Eq. (46), or the E, A, B, C path as in Eq. (47). The first way is the least computationally intensive, as it involves fewer terms.

$$\boldsymbol{p}_c = R_y(-\alpha_3)\, R_z(-\theta_4)\, R_y(-\alpha_4)\, R_z(-\theta_5)\, \boldsymbol{k} \tag{46}$$

$$\boldsymbol{p}_c = R_y(\alpha_2)\, R_z(\theta_2)\, R_y(\alpha_1)\, R_z(\theta_1)\, R_y(\alpha_5)\, \boldsymbol{k} \tag{47}$$

Figure 5(a) shows a model of the metamorphic palm and the spherical triangles used to compute its kinematics. The palm of the hand, is projected on the surface of a unit sphere. This projection preserves generality since only angles are considered. The angles θ_2, θ_3, and θ_4 are calculated by combining the coloured angle segments shown, according to Eqs. (27)–(32).

https://doi.org/10.1017/S0263574715000399 Published online by Cambridge University Press

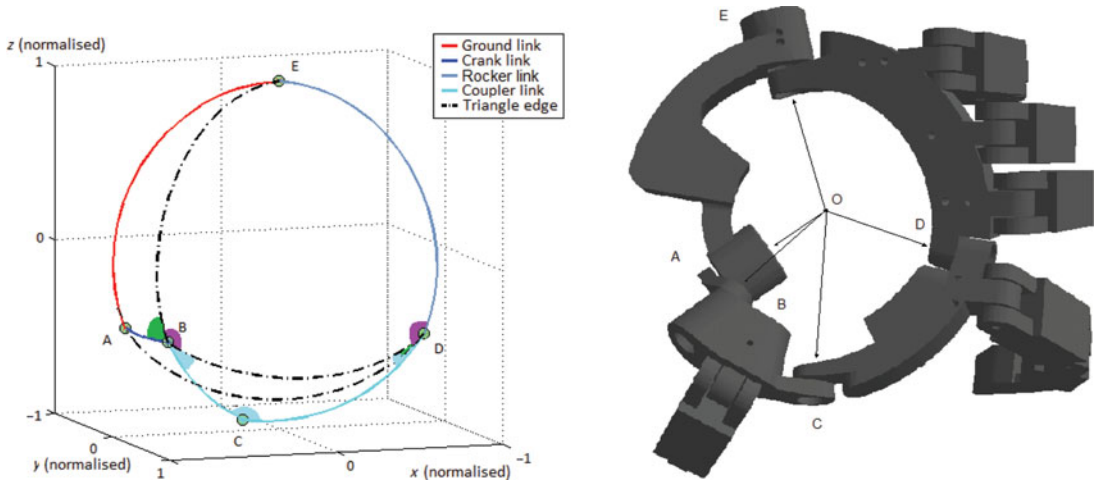

Fig. 5. Metamorphic palm triangles. (a) Computer visualisation of metamorphic palm triangles. (b) Computer rendering of the metamorphic hand.

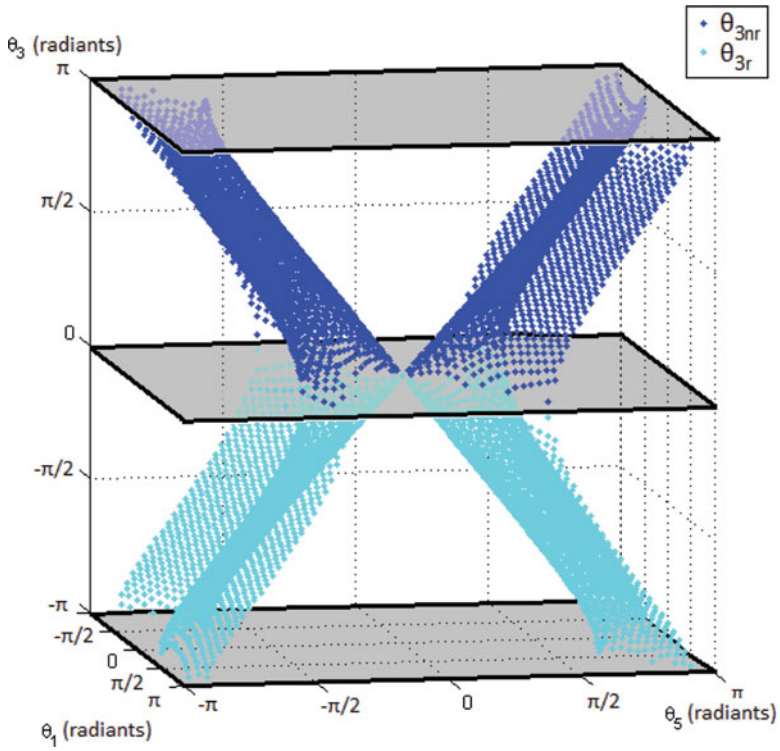

Fig. 6. Joint space of θ_3.

5.2. Joint space of the palm of the KCL metamorphic hand

Of particular interest are the joint-coupler angle θ_3 and the coupler–rocker joint angle θ_4. Figures 6 and 7 show the joint space for each joint is a manifold in a three-dimensional space where the two dimensions are the input joint angles the third dimension is the angle of the joint studied. The values for each joint are shown for both the coupler joint reflex and non-reflex configurations. It can be seen when one of the two joints is at 0°, the other input joint can only have the same value. This is the singular configuration where the palm of the hand is flat.

Figure 6 highlights the ability of the metamorphic palm to provide great flexibility in changing the relative orientations of the working planes of the index and thumb. It can be seen coupler joint angle θ_3 can reach a great number of different configurations. It is also verified the proposed method

https://doi.org/10.1017/S0263574715000399 Published online by Cambridge University Press

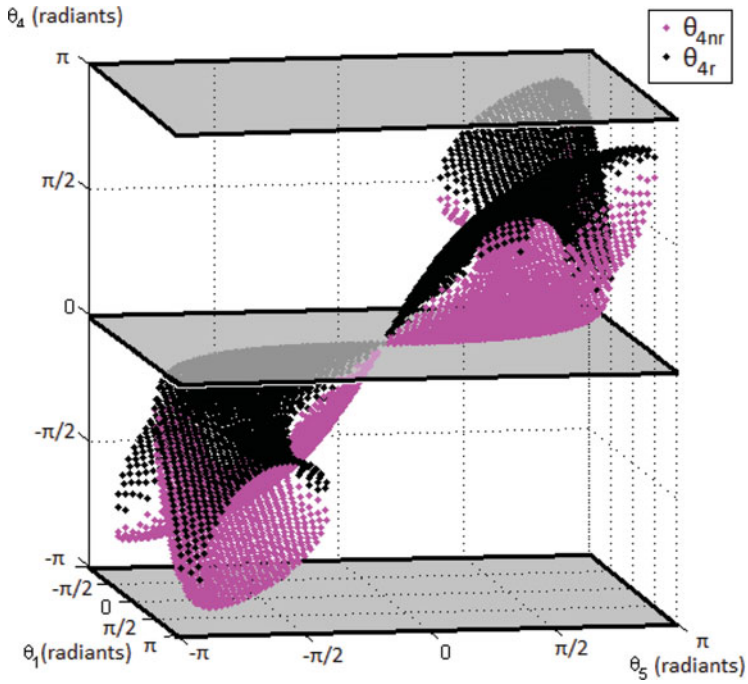

Fig. 7. Joint space of θ_4.

correctly distinguishes both reflex and non-reflex coupler joint configurations by noticing all data points of θ_{3nr} are contained in the upper half of the graph corresponding to $0 < \theta_{3nr} < \pi$ and all data points of θ_{3r} are on the bottom half corresponding to $\pi < \theta_{3nr} < 2\pi$. Finally, the planes shown in grey are where $\theta_3 = 0$ and $\theta_3 = \pi$ and the coupler joint is singular.

Figure 7 shows the rocker–coupler joint angle θ_4 is limited compared to all other joints. The planes in grey are when the joint is singular. It can be seen that joint θ_4 is singular only in the flat configuration. It is in fact the joint with the least possible attainable joint angles. This feature is desirable since collisions among fingers need to be avoided. In particular, it can be seen that rocker input joint angle θ_5 can change significantly before rocker–coupler joint angle θ_4 starts to deviate from 0 radiants so as to risk collision or significantly change the orientation of the index finger relative to the middle and little grasping fingers.

Since not all configurations are possible, when motion planning from one configuration to another, a path can be generated that lies on the surface of the joint space manifold for each joint. This path planning could be done by setting a starting point and a goal and then using a path planning algorithm on the point cloud of the appropriate joint space. Once this is done, the path can be projected onto the actuated joint plane.

6. Workspace and Visualisation of the KCL Metamorphic Multifingered Robotic Hand

6.1. Structure and geometry of a multifingered metamorphic robotic hand

Based on the concept of metamorphosis, four generation of metamorphic robotic hands are presented in Fig. 8.

Figure 8 illustrates the structure of a multifingered metamorphic robotic hand with an articulated palm. The palm is formed by a spherical five-bar linkage comprising five links denoted as l_1, l_2, l_3, l_4 and l_5 with the base link l_5 connected to a wrist that is linked to the forearm. All the fingers are mounted to the links of the articulated palm. The thumb is mounted to link l_2, the index finger is mounted to link l_3 and the rest of the fingers are mounted to link l_4. In this robotic hand, except for the thumb, each of the other fingers contain only three revolute joints with parallel axis of rotation, that provide only flexion/extension motions but no adduction/abduction motion. The introduction of the articulated palm compensates for the absence of adduction/abduction motions of the fingers and

https://doi.org/10.1017/S0263574715000399 Published online by Cambridge University Press

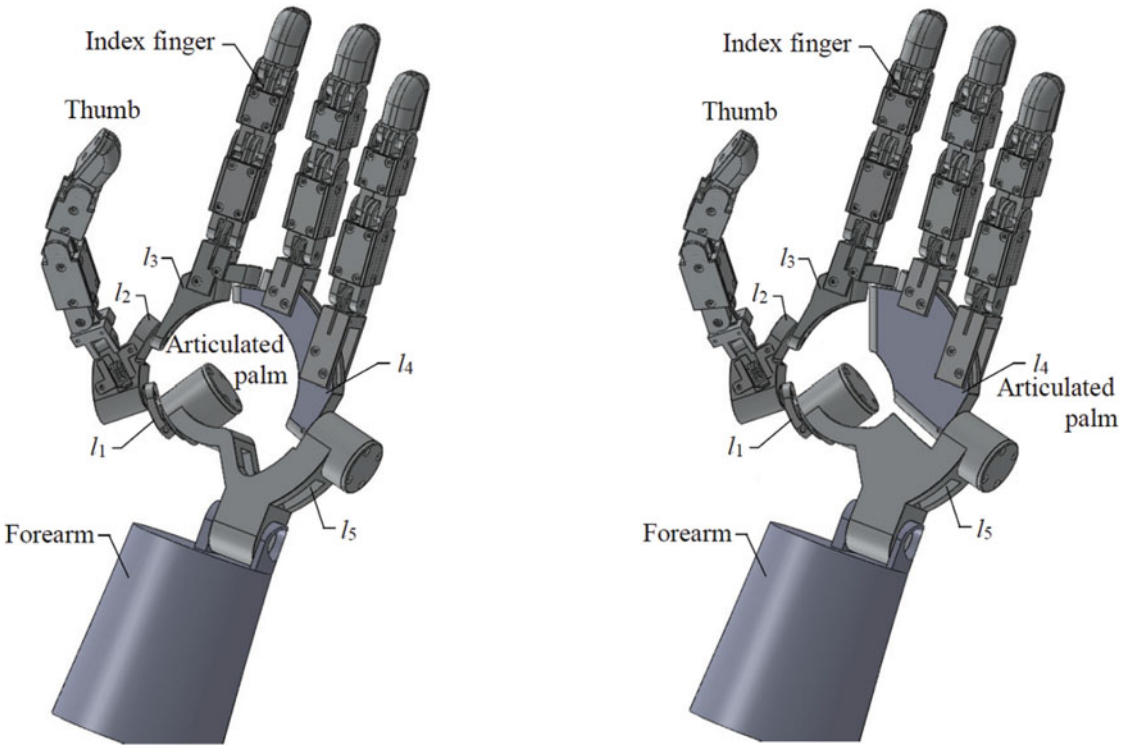

Fig. 8. A multifingered metamorphic robotic hand. (a) A metamorphic hand with hollow palm. (b) A metamorphic hand with opposable palm.

Fig. 9. Practical configurations of the metamorphic hand. (a) Origami carton folding experiment. (b) Dexterous deboning experiment.

provides dexterous manipulation and grasping capabilities by adapting the configuration of the hand for various tasks and different environments.

Figure 9 shows two practical configurations of the hand. Figure 9(a) shows a configuration of the hand for an origami carton folding experiment carried out during the EU project Topology Based Motion Synthesis (TOMSY). The sensor wires coming out of the top of the fingers are visible, as well as the tendon sheaths connected at the base of each finger on the palm. An origami-type crush-lock carton is being folded to demonstrate the dexterity of the metamorphic robotic hand. Figure 9(b) shows a configuration where the palm is not hollow to more closely resemble the biomechanical characteristics of a human palm. In this experiment, the hand is assisting a butcher during a meat de-boning operation. This is accomplished by grasping and holding pieces of beef as the butchers separates the pieces by using a knife. The gap at the centre of the palm is covered so the fingers can

https://doi.org/10.1017/S0263574715000399 Published online by Cambridge University Press

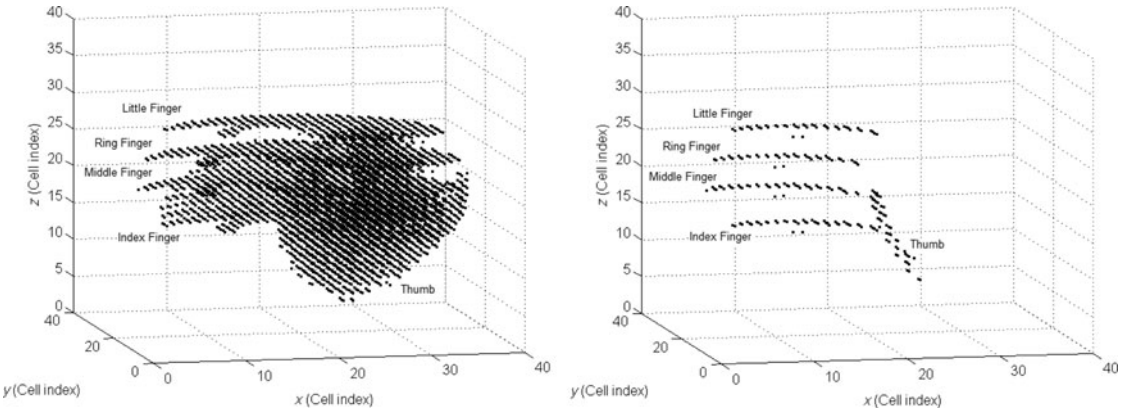

Fig. 10. Hand workspace. (a) Workspace with metamorphic palm. (b) Workspace without metamorphic palm.

oppose the body of the palm and properly grasp the beef. A glove is fitted over the hand for protection against beef fluids and prevent the entanglement of cables and tendon sheaths.

In order to increase the dexterity of the palm, both human-hand structure from the humanoid point of view and the rotatability criterion of the spherical linkage[21] from the kinematics of mechanisms point of view as well as the singularity avoidance design criteria presented in this work are considered and the angles of the links satisfy $\alpha_1 + \alpha_2 + \alpha_3 + \alpha_4 + \alpha_5 = 360^\circ$ and $\alpha_1 + \alpha_2 + \alpha_5 > \alpha_3 + \alpha_4$. The palm itself has two degrees of freedom such that two drives are used to adjust configurations of the palm with the drive adjacent to link l_1 in particular being used to change the structure of the articulated palm by rotating the crank link, i.e. link l_1, so as to form four-bar linkage in instant and innate metamorphic phases.[15]

6.2. Simulation and visualisation of the KCL metamorphic hand

To compute the workspace of the metamorphic hand, a slight variation of the method used to obtain the joint space of the spherical five-bar linkage was used. This procedure is also similar to the one found in.[29] In order to record the hand workspace, the space surrounding the hand is segmented into cells. This is done by surrounding the hand with a three-dimensional array. Each cell of the array is a 32 bit word. Each point of interest on the hand is assigned a single bit of the word. In particular, the least important half bytes are assigned to the thumb, index finger, middle finger, ring finger and little finger in that order. The bits in each half byte correspond to the ends of the metacarpal (MC), proximal (P), intermediate (I) and distal (D) phalanges for each finger. The 12 remaining bits of the word are assigned to the palm joints and the carpal metacarpal joints (CMC).

By using an array to represent the workspace, the number of points to be stored and displayed is limited to the array size. The array used in the following examples contains $40 \times 40 \times 40 = 64{,}000$ cells. If the same workspace was to be generated without the array, a much greater number of points would need to be generated and displayed. In particular, in the case where the two palm joints are swept over 180° ranges and the fingers are swept over 90° ranges, both with a 1° step, $4'212'400$ points are generated in Cartesian space. This is two orders of magnitude more points to store and draw compared to the array case. It is impractical for common math software to display this large number of points and allow the user to rotate the graph. Further, most of those points are overlapping and provide no new information to the user.

Figure 10(a) shows a visualisation of the hand's workspace with a metamorphic palm, using the workspace array method. Figure 10(b) shows the workspace of the same finger structure but with a rigid palm. The fingers are attached on the exact same spots on the palm and the palm geometry is the same. Just by examining the workspace of the index and thumb fingers and comparing it to the workspace of the same hand without an articulated palm, it becomes apparent how the metamorphic palm enhances the workspace of the hand compared to a fixed palm.

Figure 11 is a 3D rendering of the hand presented to the hand's operator by the control software. Link geometry information, in the form of triangle vertices, is imported to the software by using a custom STL file parser. A C++ library containing the kinematic equations described in this paper is used to compute palm joint angles. These computed joint angles are then used to form homogeneous

https://doi.org/10.1017/S0263574715000399 Published online by Cambridge University Press

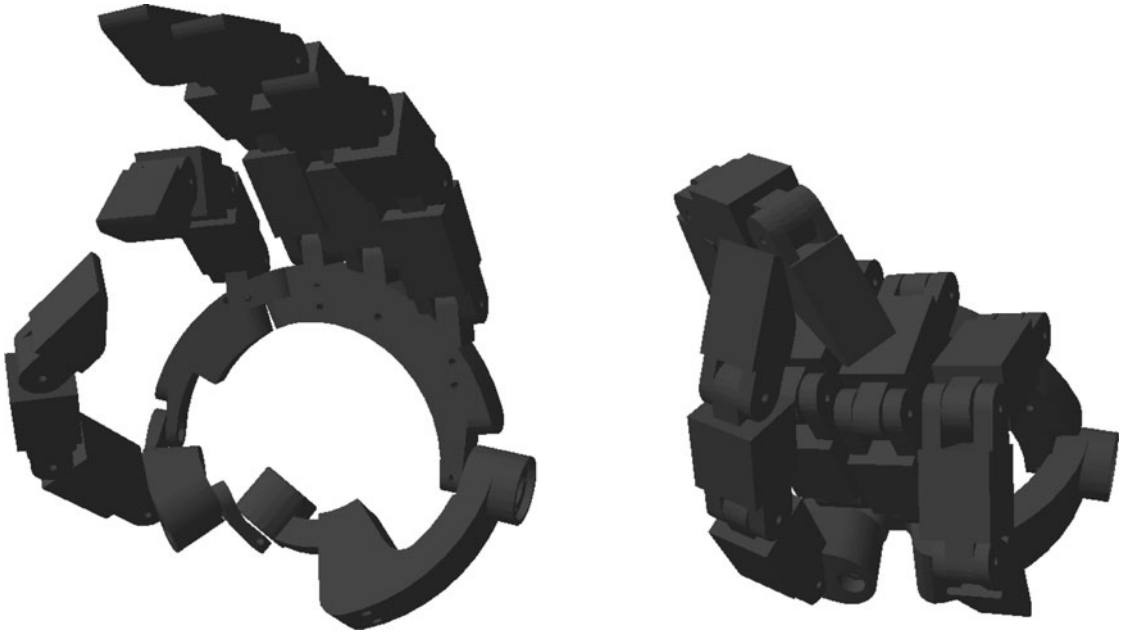

Fig. 11. Hand metamorphosis. (a) 2-DOF dexterous configuration. (b) one-DOF compact configuration.

transform matrices based on the work of Wei.[17] These homogeneous transform matrices and vertices are then fed into a standard C++ / DirectX10 pipeline to render the hand on screen.

Figure 11(a) shows the dexterous operating mode of the hand where no palm joint is singular. In this motion branch, both palm input motors affect the pose of the hand independently and the hand shows maximum dexterity. This configuration is useful for manipulating large and complex objects, including articulated objects as shown in Fig. 9(a). When the crank link α_1 folds over ground link α_5, the palm now becomes a one-DOF mechanism. One such configuration is shown in Fig. 11(b). In this configuration, the hand becomes more compact and can manipulate objects in tight spaces as well as perform grasps that are more stable since less degrees of freedom need to be controlled. In such a one-DOF configuration, however, the fingers can easily collide and as a result the possible of hand poses are limited.

6.3. Numerical examples

Table I shows numerical examples. Rocker input joint angle is limited to $\|\theta_5\| / leq 120^\circ$. Crank input joint angle is first set to $\theta_1 = 0^\circ$ then to $\theta_1 = 180^\circ$ to first show the home configuration, then to show the one-DOF compact configuration.

The symmetry of the coupler joint angle θ_{3nr} can be verified when rocker input joint angle θ_5 is changed to be reflex and non-reflex. Another feature particular to the non-reflex coupler joint configuration is when $\theta_1 = 0$, the crank coupler joint angle θ_{2nr} and the rocker–coupler joint angle θ_{4nr} change very slightly while coupler joint angle θ_{3nr} is almost equal to the rocker input angle θ_5. This is because of the decision to be $\alpha_1 + \alpha_2 + \alpha_5 \approx \alpha_3 + \alpha_4 \approx \pi$ in this particular design.

Table II shows inverse kinematics numerical examples. The coupler joint angle θ_3 and the rocker–coupler joint angle θ_4 are given. For ease of comparison, the values are drawn from the first five rows of Table I. Then, as described in Section 3.4, a cyclic permutation of the dimensions of every link is performed and the problem is solved with the value of the permuted θ_1 corresponded to θ_4 of Table I and the value for the permuted θ_5 corresponded to θ_3 of Table I. After the computations, the mechanism joint angles are remapped following the inverse cyclic permutation and the results are presented in Table II. The small numerical deviations are due to the rounding of the values of the permuted input joints to the second digit. This cross-validation procedure was also used during the development of the method to insure correctness.

Figure 12 shows four example grasps with corresponding palm joint angle values. In the first two cases, the crank link is kept flat with the ground link, and the rocker link is set to $\theta_5 = -30^\circ$

https://doi.org/10.1017/S0263574715000399 Published online by Cambridge University Press

Table I. Forward kinematics numerical examples.

θ_5	θ_1	θ_{2nr}	θ_{3nr}	θ_{4nr}
		(deg)		
0	0	0	0	0
30	0	−1.22	30.59	0.87
60	0	−2.64	61.29	1.88
90	0	−4.61	92.25	3.28
120	0	−8.15	123.98	5.8
90	180	−169.15	62.12	58.13
120	180	153.1	107.05	62.55
−120	180	28.01	107.05	−148.87
−90	180	56.79	62.12	127.4

Table II. Inverse kinematics numerical examples.

θ_{3nr}	θ_{4nr}	θ_5	θ_1	θ_{2nr}
		(deg)		
0	0	0	0	0
30.59	0.87	29.99	0	−1.22
61.29	1.88	60.00	−0.01	−2.64
92.25	3.29	90.00	0	−4.61
123.98	5.80	120.00	−0.01	−8.15

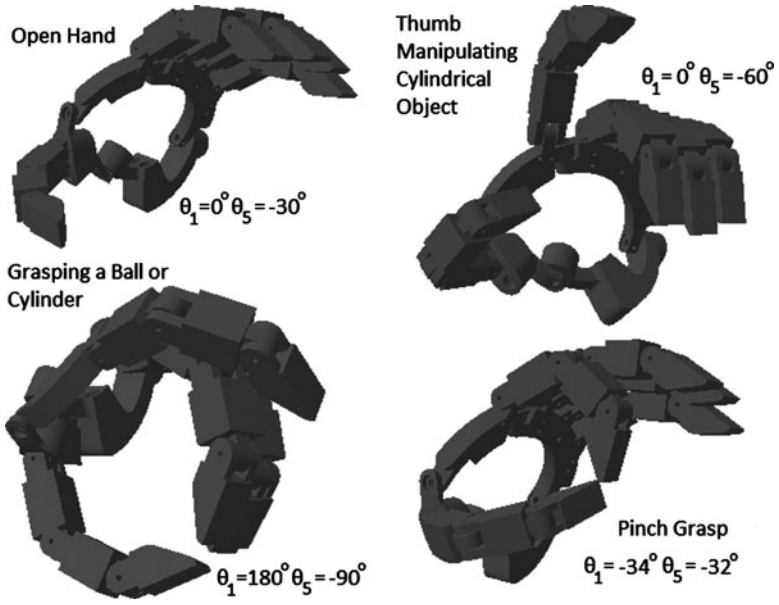

Fig. 12. Grasp examples.

and $\theta_5 = -60^\circ$ respectively. In the -30° configuration, the hand is very open and this can be used to manipulate large objects, like panels of origami cartons or buttons on a device. In the -60° configuration, the palm is folded significantly and here in particular the grasping fingers form a cylindrical grasp and the thumb is free to manipulate the top of the cylindrical object being grasp, such as the nozzle of a spray can. In the third configuration, it is $\theta_1 = 180^\circ$ and $\theta_5 = -90^\circ$. In this configuration, the crank is fully folded and the rocker link is at such an angle to allow the full folding of the crank and position the grasping fingers so the thumb can oppose them. This configuration is useful for performing a tight grip around a small object such as a small ball or cup filled with a beverage. Notice the index finger has to be positioned in such a way as to avoid collision with the

https://doi.org/10.1017/S0263574715000399 Published online by Cambridge University Press

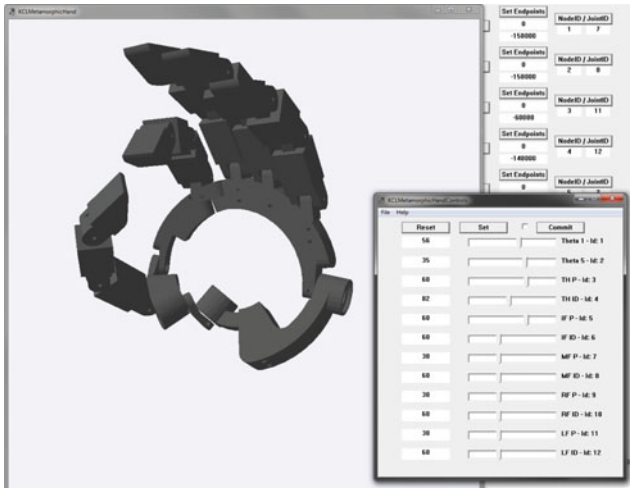

Fig. 13. Hand control user interface.

middle finger. The fourth configuration shown has $\theta_1 = -34^\circ$ and $\theta_5 = -32^\circ$ and shows a pinch grasp with the palm slightly curved to the inside to resemble a more natural, human-like appearance, similar to the gesture commonly associated with the English work "OK", which is a word usually denoting approval or acknowledgment.

7. Application

The results presented in this paper have been used in the user interface of the control software of the five-fingered version of the KCL Metamorphic Hand. In terms of computational effort, a C++ implementation on a Windows 7 desktop computer with an Intel Core2 6420 running at 2.13 GHz is able to complete one full computation of the forward kinematics in 234 μs. By further optimising the code to reuse variables and use direct memory addressing, the execution time was dropped to 117 μs.

Figure 13 shows a screenshot of the control software user interface. It consists of three windows. The main window contains sliders to set the joint angles for the palm and hand. The user can either manipulate the sliders, or type in the desired angle value for each joint and press the "Set" button. The "Reset" button resets the hand to the home configuration. The user then looks at the second window showing a visualisation of the hand with the selected joint angles. The visualisation is generated by using the Direct3D libraries, the kinematics functions presented in this paper and imported vertex data from CAD STL files. If the pose of the hand is satisfactory, the user can press the "Commit" button on the first window in order to send the commands to the motors. The third window presents information related to the control thread of the program such as terminal values for each motor and the motor nodeID to hand joint map.

8. Conclusions

Spherical trigonometry was used for computing the direct and inverse kinematics of spherical five-bar linkages, as well as the direct kinematics of the KCL metamorphic robotic hand. The spherical palm is segmented into spherical triangles which are then solved and their angles combined to fully solve the palm configuration. The presented method allows differentiation of coupler joint reflex and non-reflex configurations. The same set of equations can be used for both forward and inverse kinematics, just by a simple cyclic permutation of the joint and link numbers.

By using spherical trigonometry, singularities become obvious by inspecting the equations of the angles of each spherical triangles the palm is decomposed into. Singularity-avoidance based design criteria were presented. Point clouds were generated that represent the joint space of the palm. The joint space as well as the work space point clouds were generated and stored in a computer using an efficient method of segmenting the workspace into 32 bit word cells with each bit of each cell encoded a different point of interest of the hand. This allows displaying the hand's workspace on

https://doi.org/10.1017/S0263574715000399 Published online by Cambridge University Press

demand without the need to re-compute it. Comparison of the hand with a metamorphic palm and a fixed palm was made and two examples of the two-DOF dexterous configuration and the one-DOF compact configuration were shown that highlight the advantage of an articulated palm equipped metamorphic hand.

Acknowledgements

The authors gratefully acknowledge the support from the European Commission 7th Framework Program Squirrel under Grant No. 610532.

References

1. C. Melchiorri and M. Kaneko, "Robot Hands," **In**: *Springer Handbook of Robotics* (Bruno Siciliano, Oussama Khatib, eds.) (Springer, New York, NY, 2008) pp. 345–360.
2. G. A. Bekey, T. Rajko and Z. Ilija, "Control architecture for the belgrade/usc hand," *Dextrous Robot Hands* 136–149 (1990) (http://www.springer.com/gp/book/9781461389767).
3. J. Butterfass, M. Grebenstein, H. Liu and G. Hirzinger, "Dlr-hand II: Next Generation of a Dextrous Robot Hand," *Proceedings of 2001 IEEE International Conference on Robotics and Automation*, Seoul, Korea, vol. 1 (2001) pp. 109–114.
4. R. Ambrose, H. Aldridge, R. Askew, R. Burridge, W. Bluethmann, M. Diftler, C. Lovchik, D. Magruder and F. Rehnmark, "Robonaut: Nasa's Space Humanoid," *Intell. Syst. Appl.* **15**(4), 57–63 (2000).
5. C. S. Lovchik and A. D. Myron, "The Robonaut Hand: A Sexterous Robot Hand for Space," *Proceedings of 1999 IEEE International Conference on Robotics and Automation*, Detroit, Michigan, USA, vol. 2 (1999) pp. 907–912.
6. R. Walker, "Design of a Dextrous Hand for Advanced Clawar Applications," *Conference Documentation of the 6th International Conference on Climbing and Walking Robots (CLAWAR)* (2003) pp. 17–19.
7. W. Townsend, "The barrett hand grasper-programmably flexible part handling and assembly," *Indust. Robot: Int. J.* **27**, 181–188 (2000).
8. G. Carbone and M. Ceccarelli, "Design of Larm Hand: Problems and Solutions," *IEEE International Conference on Automation, Quality and Testing, Robotics, 2008. AQTR*, vol. 2 (2008) pp. 298–303.
9. C. Yao, Z. Qiang, M. Ceccarelli, G. Carbone, Y. Shuangji and L. Zhen, "Design and Simulation of a dsp Controller for a Larm Hand," *Proceedings of the 2nd International Asia Conference on Informatics in Control, Automation and Robotics (CAR)*, Wuhan, China, vol. 1 (2010) pp. 361–364.
10. F. Lotti, P. Tiezzi, G. Vassura, L. Biagiotti, G. Palli and Melchiorri, C. "Development of ub Hand 3: Early Results," *Proceedings of the 2005 IEEE International Conference on Robotics and Automation*, Barcelona, Spain, (2005) pp. 4488–4493.
11. G. Palli, U. Scarcia, C. Melchiorri and G. Vassura, "Development of Robotic Hands: The ub Hand Evolution," *IEEE/RSJ International Conference on Intelligent Robots and Systems (IROS)* (2012) pp. 5456–5457.
12. H. Liu, K. Wu, P. Meusel, N. Seitz, G. Hirzinger, M. H. Jin, Y. W. Liu, S. W. Fan, T. Lan and Z. P. Chen, "Multisensory Five-Finger Dexterous Hand: The dlr/hit Hand ii," *IEEE/RSJ International Conference on Intelligent Robots and Systems, IROS 2008.* (2005) pp. 3692–3697.
13. C. Dongmin, S. Seunghoon, K. Ja Choon, C. Hyouk Ryeol and M. Hyungpil, "The SKKU Hand: Work in Progress," *Proceedings of the 9th International Conference on Ubiquitous Robots and Ambient Intelligence (URAI)*, Daejeon, Korea, (2012) pp. 437–438.
14. J. S. Dai, Robotic hand with palm section comprising several parts able to move relative to each other, WO/2005/105391, (Nov. 10, 2005) (International Patent No. PCT/GB2005/001665 and UK Patent No. GB04 095 48.5).
15. J. S. Dai and D. Wang, "Geometric analysis and synthesis of the metamorphic robotic hand," *J. Mech. Des.* **129**(11), 1191–1197 (2007).
16. J. S. Dai, D. L. Wang and L. Cui, "Orientation and workspace analysis of the multifingered metamorphic hand – metahand," *IEEE Trans. Robot.* **25**(4), 942–947 (2009).
17. G. Wei, J. S. Dai, S. Wang and H. Luo, "Kinematic analysis and prototype of a metamorphic anthropomorphic hand with a reconfigurable palm," *Int. J. Humanoid Robot.* **08**(03), 459–479 (2011).
18. J. S. Dai and J. R. Jones, "Mobility in metamorphic mechanisms of foldable/erectable kinds," *J. Mech. Des.* **121**(3), 375–382 (1999).
19. J. S. Dai and J. R. Jones, "Matrix representation of topological changes in metamorphic mechanisms," *J. Mech. Des.* **127**(4), 837–840 (2005).
20. G. Wei and J. S. Dai, "Origami-inspired integrated planar-spherical overconstrained mechanisms," *J. Mech. Des. Trans. ASME* **136**(5), 051003 (2014).
21. Y. Liu and K. L. Ting, "On the rotatability of spherical n-bar chains," *Trans. ASME: J. Mech. Des.* **116**(9), 920–923 (1994).
22. C. M. Gosselin and J. F. Hamel "The Agile Eye: A High-Performance Three-Degree-of-Freedom Camera-Orienting Device," *Proceedings of IEEE International Conference on Robotics and Automation*, San Diego, CA, USA, (1994) pp. 781–787.

23. C. W. Wampler, "Displacement analysis of spherical mechanisms having three or fewer loops," *ASME J. Mech. Des.* **126**, 93–100 (2004).
24. J. M. McCarthy, *Geometric Design of Linkages* (Springer, New York, NY, 2000).
25. K. C. Gupta and A. S. Beloiu, "Branch and circuit defect elimination in spherical four-bar linkages," *Mechanism* **33**(5), 491–504 (1998).
26. C. H. Chiang, *Kinematics of Spherical Mechanisms* (Krieger Pub Co., Malabar, Florida, USA, 2000)
27. J. Duffy, *Analysis of Mechanisms and Robot Manipulators* (1980).
28. L. Cui and J. S. Dai, "Posture, workspace, and manipulability of the metamorphic multifingered hand with an articulated palm," *J. Mech. Robot. Trans. ASME* **3**(2), 021001 (2011).
29. M. Ceccarelli, *Fundamentals of Mechanics of Robotic Manipulation* (Kluwer/Springer, New York, NY, 2004).